

DEVELOPMENT OF ANTHROPOMORPHIC DUAL ARM ROBOT WITH DISTINCT DEGREES OF FREEDOM FOR COORDINATED OPERATIONS

Submitted: 2nd July 2019; accepted: 20th December 2019

Abhaykrishna K M, Nidhi Homey Parayil, Ibin Menon Reghunandan, Sudheer A P

DOI: 10.14313/JAMRIS/4-2019/38

Abstract: *Development of assistive robots for helping the disabled is a field of research that has gathered attention recently. According to surveys, about one billion people in the world population have some kind of disability. Dual arm robots are a suitable solution for helping people with mobility impairments. The current development in the field of dual-arm robots is focused mainly in the industrial field to carry out cyclic tasks. This includes activities such as pick and place, assembling parts and doing other industrial operations. Unlike human arms, these dual arm robots lack versatility in doing a wide variety of tasks with adequate coordination between the arms. Due to these constraints, industrial dual arm robots cannot be directly implemented for assisting the disabled. This paper focuses on designing a compact dual arm robot which closely mimics human arms to do coordinated tasks with lesser Degrees of Freedom (DoF). Therefore, the developed robot extends its capabilities from industrial applications to daily life activities. Closed loop control is used in actuating the proposed 9 DoF dual arm robot with distinct DoF. Target position is acquired using image processing. Hand to hand coordination in various operations such as pick and place, transferring objects, serving food, etc. has successfully experimented.*

Keywords: *Dual arm robot, Anthropomorphic ratio, Distinct Degrees of Freedom, Coordination, Object detection*

1. Introduction

In recent years, there has been a growing interest in the field of robot based coordination. It has huge potential applicability in fields like industry, medical services and rehabilitation. As humans have a complex brain structure with well-developed neural network architecture, their ability to control and coordinate arm motions are highly accurate and advanced. Dual robotic arm can be used for imitating the human arm motions for doing such coordinated tasks for various applications in manufacturing and service industries. Dual arm robots are basically a combination of two robotic arms attached to the same base that can replicate coordinated tasks.

Dual arm robots can achieve a wide variety of tasks similar to human hands. It can do multiple tasks and consumes less space compared to two independent manipulators [1]. Dual arm robots can approach a target in various angles and it requires less cycle time compared to single arm robots. Current practice is to increase the Degrees of Freedom (DoF) to achieve complex tasks of the manipulator robot. As the number of DoF increases, robot control becomes difficult due to redundancy. It will also increase the energy requirement and cost, as the number of actuators is high.

Terak *et al.* [1] proposed the design and control of a 7 DoF dual arm robot and discussed the importance of arms for the stability of the robot. The design comprised of a rotating torso and two 3 DoF arms, aiming to achieve the best performance in terms of dynamic balance but the feasibility to do coordinated tasks is not taken into account. Moreover, the implementation of coordination between the two arms was not achieved. Banerji *et al.* [2] proposed a systematic approach to judge the feasibility of wrist joint ranges and to find reasonable target trajectories or orientations. Though cooperative tasks were achieved, the project used two separate individual manipulators which require larger space compared to a dual arm robot. In the study proposed by Tsarouchi *et al.* [3], benefits of using of dual arm robot in an assembly line were analysed and concluded that the workstation setup increased the workspace and simplified the programming. Most of the dual arm robots he analysed are bulky and designed for specific applications as they are used in the industries. Huang *et al.* [4] developed a collision model of a dual arm robot used for rehabilitation of hemiplegic patients. Safety was guaranteed by including passive compliance but the performance was compromised. An innovative design of 8 DoF dual arm robot with the tilted shoulder is presented by Lee *et al.* [5]. Though the proposed design increased manipulability of the robot, redundancy issues prevail. The dual arm robot developed by Park *et al.* [6] is designed for doing assembly operations in industries. The robot is capable to do multiple coordinated tasks in industrial applications but as the design is bulky its application to the household is limited. YuMi developed by ABB was the world's first truly collaborative dual-arm robot. It is equipped with dual-arms, flexible hands, universal parts feeding system, camera-based part location, lead-through programming and precise motion control [7].

Majority of the models proposed in the literature have redundancies due to the increased degrees of freedom. Moreover, the cost of the robots used and those fabricated for studies are considerably high. Most of the dual-arm robots are task specific as they are designed for industrial applications and their size is considerably high. Their design does not mimic the human arm and hence the extent of their application to do household activities is limited. Furthermore, coordination has not been given enough importance in the case of industrial dual-arm robots. A dual arm robot with human-like or anthropomorphic design provides more flexibility to mimic the household tasks such as feeding, opening a bottle and picking objects which in turn can be used to replace caretakers to help the disabled. This paper aims at designing and developing an anthropomorphic dual-arm robot that is compact, low cost and capable of multitasking with minimum degrees of freedom. Furthermore, the implementation of coordination between the arms is tested for applicability in assisting disabled people.

2. Modelling of Dual Arm Robot

This section deals with the conceptual design of the dual arm robot followed by kinematic modelling using anthropomorphic link dimensions, static structural analysis, dynamic modelling and trajectory planning. The conceptual design of the dual arm robot is shown in Fig. 1.

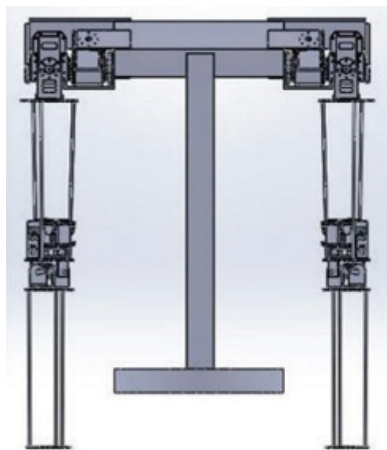


Fig. 1. Conceptual design of dual arm robot

2.1. Kinematic Modelling

In order to obtain human-like characteristic motion, all DoF are chosen to be revolute. The robot developed has four DoF on the left arm and five DoF on the right arm. This configuration with less DoF leads to less energy consumption, easier control and low cost. Joint DoF are assigned as shown in Table 1.

The dual arm robot is designed as two independent serial link manipulators that are fixed to a T shaped base. Novel changes at shoulder and elbow joints are implemented to make the robot sufficiently dextrous in the common workspace to orient both

arms for doing coordinated tasks. In order to increase the workspace in the upper area of the transverse plane, the shoulder support is tilted by 45 degrees upwards about the coronal plane as shown in Fig. 2.

Tab. 1. Joint DoF of dual arm robot

Joint	Right hand		Left hand	
	No of DoF	Type of motion	No of DoF	Type of motion
Shoulder	2	Pitch & Yaw	2	Pitch & Yaw
Elbow	1	Pitch	1	Pitch
Wrist	2	Roll & Pitch	1	Roll

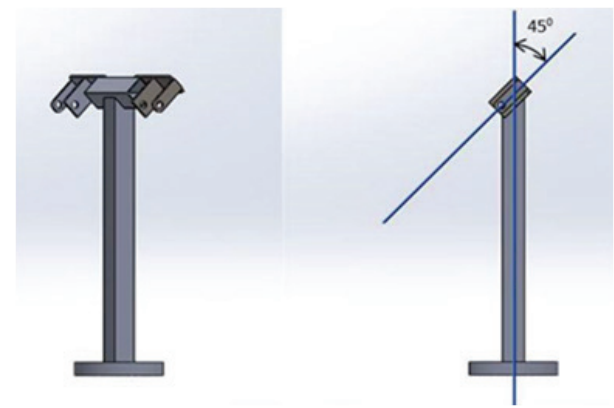


Fig. 2. Joint tilts at shoulder

Tab. 2. Dimensions of dual arm robot

Robot links	Length in mm
Shoulder	314.6
Upper arm	226.8
Forearm	178
Wrist	131.7

The elbow joint axis is inclined at 45 degrees inwards with respect to the shoulder yaw axis as shown in Fig. 3 so as to maximize the common workspace between the arms.

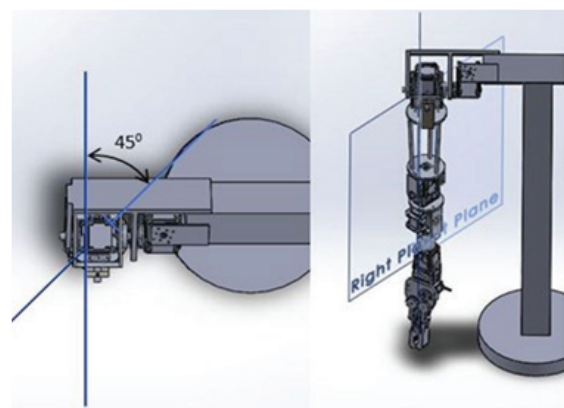


Fig. 3. Joint tilts at the elbow

The dimensions of the links of dual arm robot are calculated using anthropomorphic ratios of a human body [8] for a reference human height of 1220mm and are shown in table 2.

Denavit Hartenberg (D-H) convention is used for kinematic modelling [9]. Coordinate frames are assigned to each joint as shown in Fig. 4.

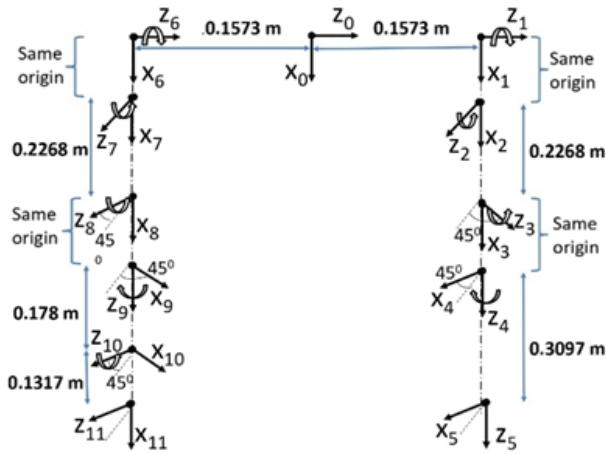


Fig. 4. Frame assignment of joints in the dual arm robot

D-H parameters for right and left arms are formulated and are shown in table 3 and table 4 respectively. Forward Kinematics is used to find the position and orientation of the end-effector with respect to a reference frame when joint variables are known. The pose of *i*th frame in terms of D-H parameters is obtained from standard homogenous transformation matrix. The final transformation matrix of each arm is found by multiplying the individual transformation matrices of joints for the corresponding arm.

in the user-defined upper and lower bounds of *x*. In the trust region method, the function *f* is approximated to a simpler function *q*, that imitates the behaviour of the function *f* in a neighbourhood *N* around *x*, called the trust region. The trust-region subproblem is to compute a trial step *s* by minimizing *q* over trust-region *N*. Once trial step *s* is computed, if *f(x+s)* is less than *f(x)*, then *x* is changed to *x + s* and steps are repeated. If the condition is not satisfied, *x* would remain unchanged and the size of the trust space is reduced. The flow chart of this algorithm is as shown in Fig. 5.

Tab. 3. DH Parameters of the right arm

Link	θ (deg)	D(m)	a(m)	α (deg)
1(Base)	0	-0.1573	0	0
2	θ_1	0	0	90
3	θ_2	0	0.2268	45
4	$\theta_3 + 90$	0	0	90
5	θ_4	0.178	0	-90
6	$\theta_5 - 90$	0	0.1317	0

Tab. 4. DH Parameters of the left arm

Link	θ (deg)	D(m)	a(m)	α (deg)
1(Base)	0	0.1573	0	0
2	θ_1	0	0	90
3	θ_{12}	0	0.2268	-45
4	$\theta_3 - 90$	0	0	-90
5	θ_4	0.3097	0	0

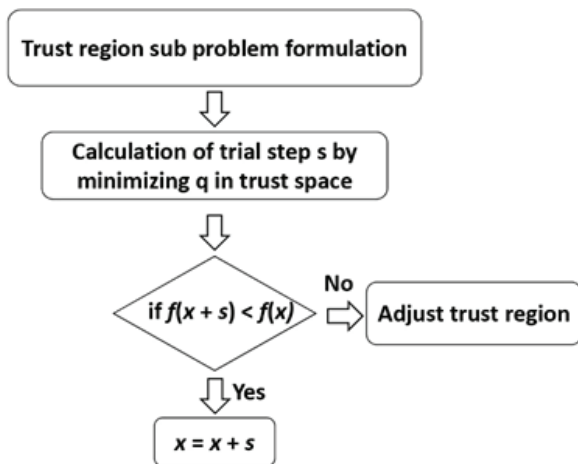


Fig. 5. Trust region method

The joint variables are obtained from the given pose of the end-effector using inverse kinematics. It is calculated by equating the final transformation matrices to the desired end-effector pose. The non-linear equations in inverse kinematics are solved in MATLAB iteratively using lsqnonlin, which is a nonlinear least-squares solver. lsqnonlin uses the iterative trust-region reflective algorithm [10] for optimizing a function *f(x)*

2.1.1. Novel Gripper Design

A windshield wiper inspired gripper is designed that is capable of holding objects of various shapes. Furthermore, the gripping surface is made wider to increase the area of contact. The rubber padding on the gripping links ensures better grasping. The CAD model of the gripper is shown in Fig. 6.

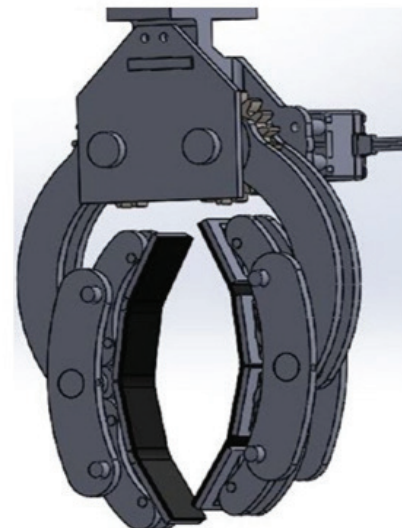


Fig. 6. CAD Model of Gripper

A CAD model is made from the anthropomorphic dimensions and other design constraints using Solid-Works. CAD model for the dual arm robot is shown in Fig. 7.

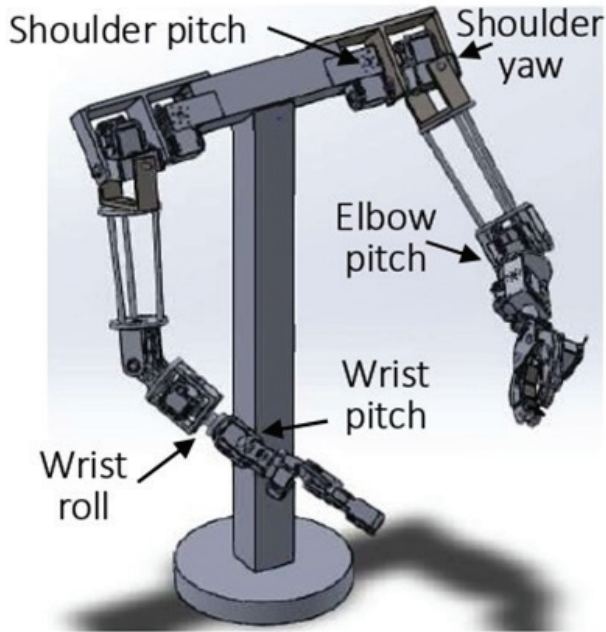


Fig. 7. CAD Model of dual arm robot

The base is made up of rigid square bars. A skeleton-like structure is designed for the upper arm. Bearing housings are specifically designed for shoulders to accommodate multiple DoF. Tapering is provided for the upper arms to make it more human-like.

2.2. Static Structural Analysis

Static analysis is used to optimize the design by determining the stresses and deformation developed in the robot links due to static forces. In this section, static analysis is carried out in ANSYS R18.2 to find Von Mises stresses [11] for a given payload at the end effector. A payload of 0.5kg is applied at gripper of the robot arm and the weights of the motors are applied at respective joints during the analysis. After assigning material properties of Aluminium and Mild steel to the CAD model, part dimensions are optimised. Yield strength of Aluminium is 276MPa and yield strength of Mild steel is 250MPa.

It is found from the static structural analysis that the induced stresses in all parts of the robot are very much less than the yield stresses of the corresponding material. Maximum stress developed among Aluminium parts is 19 MPa and among Mild steel parts is 10.8 MPa. It ensures a factor of safety above 10 with a maximum deflection of 0.18 mm at the forearm, which is within the acceptable range. Hence all subsystems are safe in design. Fig. 8 shows the static analysis results for each part.

2.3. Dynamic Modelling

In dynamic analysis, the joint torque equations are formulated in terms of joint angle, joint velocity and acceleration. In this section, the joint torque at the shoulder is calculated for horizontal arm configuration where the required torque is maximum. Lagrangian-Euler (L-E) method is used to find the joint torque equations. Lagrangian is defined as the difference of total kinetic and potential energy of the robot system. The generalised torque τ_i at joint i is calculated from the equation (1), where the parameters are obtained for each link from equations (2)-(7) [9]. The terms q_i , \dot{q}_i , \ddot{q}_i are displacement, velocity and acceleration of joint i respectively. M_{ij} represents the inertia and h_{ijk} represents velocity induced reaction torque at joint i . G_i is the gravity loading force at joint i .

$$\tau_i = \sum_{j=1}^n M_{ij}(\mathbf{q})\ddot{q}_j + \sum_{j=1}^n \sum_{k=1}^n h_{ijk} \dot{q}_j \dot{q}_k + G_i \quad \text{for } i = 1, 2, \dots, n \quad (1)$$

$$\mathbf{Q}_j = \begin{bmatrix} 0 & -1 & 0 & 0 \\ 1 & 0 & 0 & 0 \\ 0 & 0 & 0 & 0 \\ 0 & 0 & 0 & 0 \end{bmatrix} \quad (2)$$

$$\mathbf{d}_{ij} = \begin{cases} {}^0\mathbf{T}_{j-1}\mathbf{Q}_j^{j-1}\mathbf{T}_i & j \leq i \\ \mathbf{0} & j > i \end{cases} \quad (3)$$

$$\mathbf{M}_{ij} = \sum_{p=\max(i,j)}^n \text{Tr}[\mathbf{d}_{pj}\mathbf{I}_p\mathbf{d}_{pi}^T] \quad (4)$$

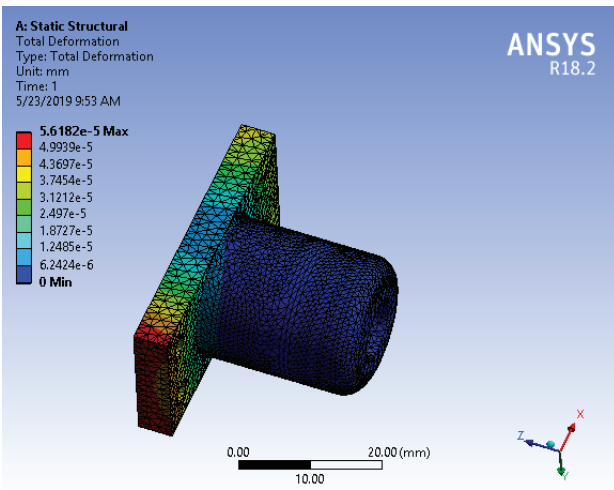
$$h_{ijk} = \sum_{p=\max(i,j,k)}^n \text{Tr} \left[\frac{\partial (d_{pk})}{\partial q_p} \mathbf{I}_p \mathbf{d}_{pi}^T \right] \quad (5)$$

$$G_i = -\sum_{p=i}^n m_p g d_{pi}^p \bar{r}_p \quad (6)$$

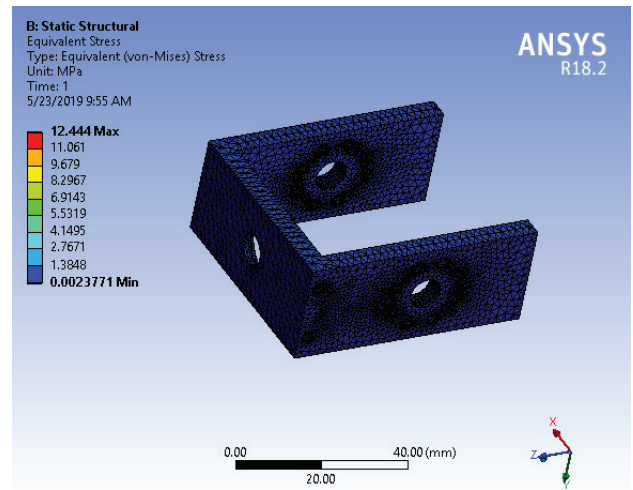
$$\frac{\partial d_{ij}}{\partial q_k} = \begin{cases} {}^0\mathbf{T}_{j-1}\mathbf{Q}_j^{j-1}\mathbf{T}_{k-1}\mathbf{Q}_k^{k-1}\mathbf{T}_i & \text{for } i \geq k \geq j \\ {}^0\mathbf{T}_{k-1}\mathbf{Q}_k^{k-1}\mathbf{T}_{j-1}\mathbf{Q}_j^{j-1}\mathbf{T}_i & \text{for } i \geq j \geq k \\ 0 & \text{for } i < j \text{ or } i < k \end{cases} \quad (7)$$

2.4. Trajectory Planning

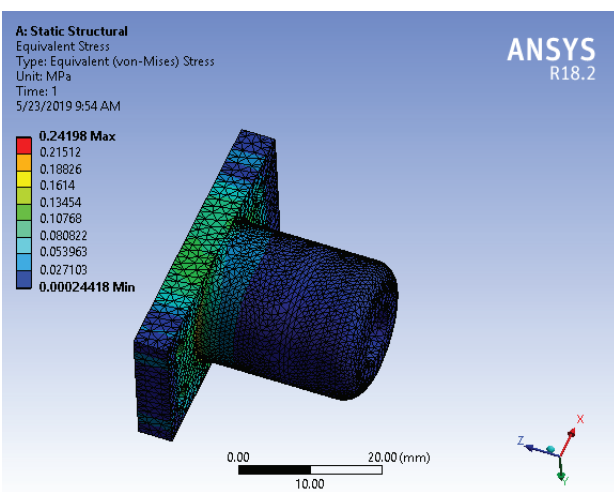
Trajectory planning describes the motion of the robot in the 3-dimensional workspace, in terms of position, velocity and acceleration [12]. In order to obtain a smooth motion, triangular velocity profile is used which gives a parabolic blend curve for angle variation with respect to time. The desired variation of joint angle, velocity and acceleration are shown in Fig. 9.



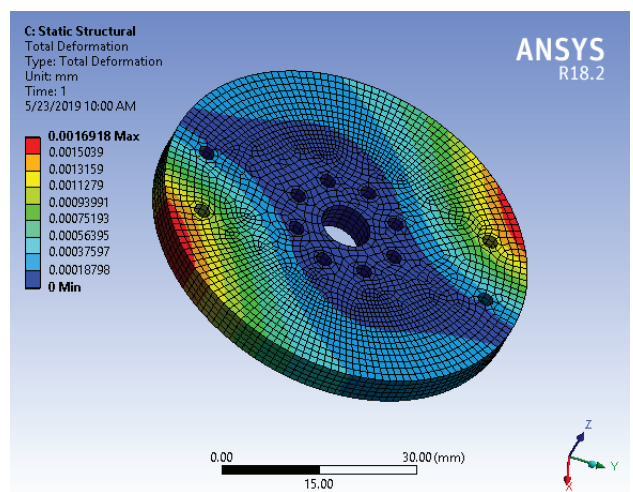
(a) Deformation of roll joint coupling



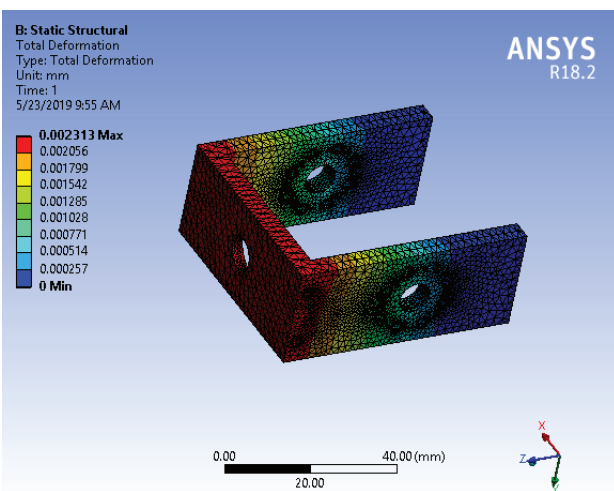
(d) Equivalent stress of roll joint housing



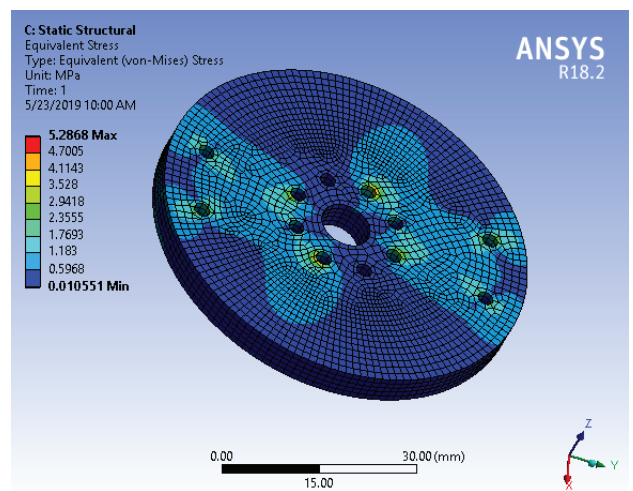
(b) Equivalent stress of roll joint coupling



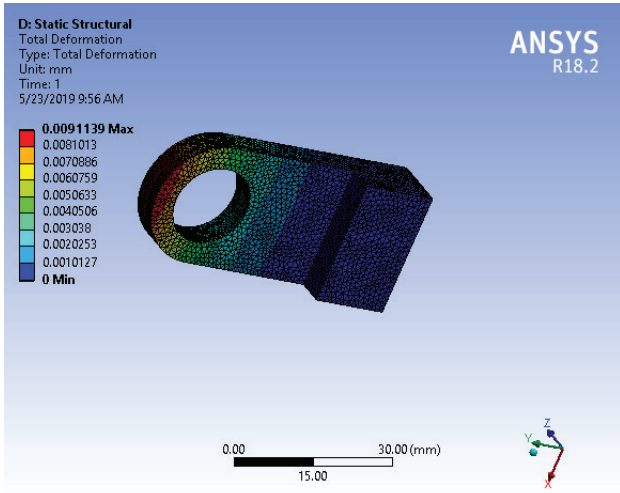
(e) Deformation of elbow plate



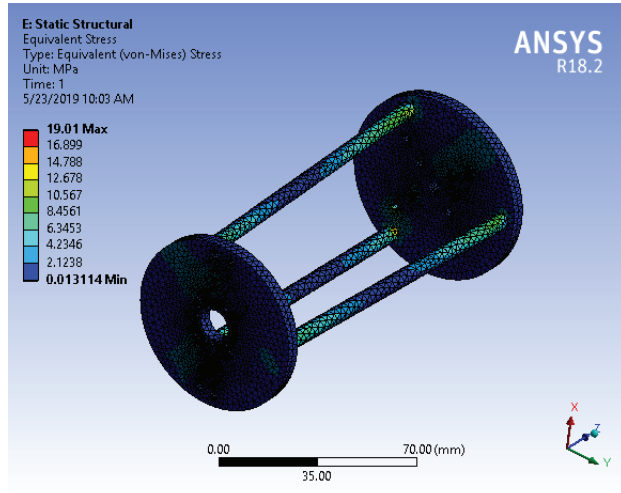
(c) Deformation of roll joint housing



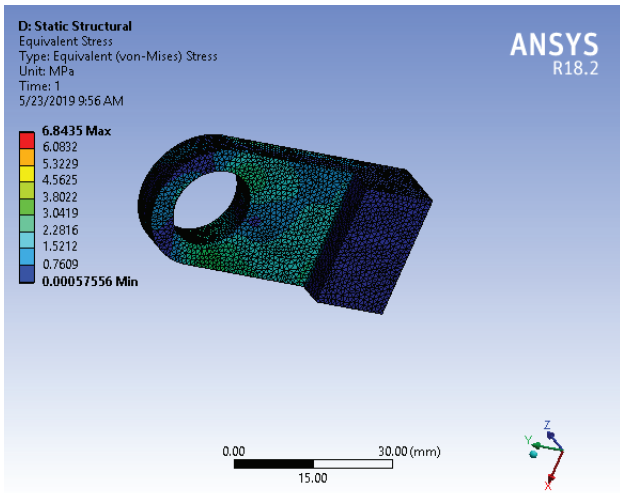
(f) Equivalent stress of elbow plate



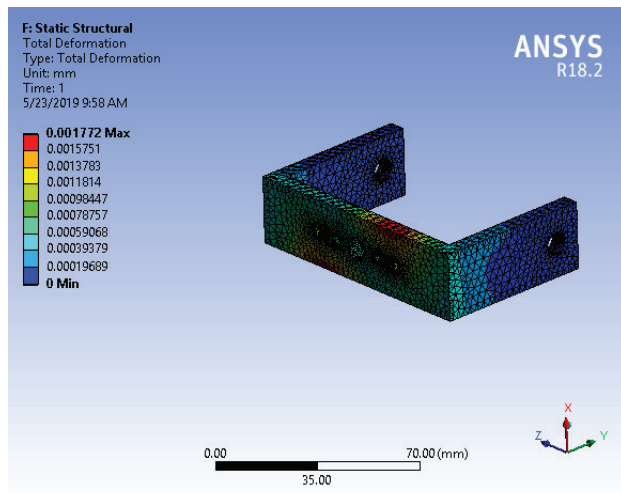
(g) Deformation of elbow housing



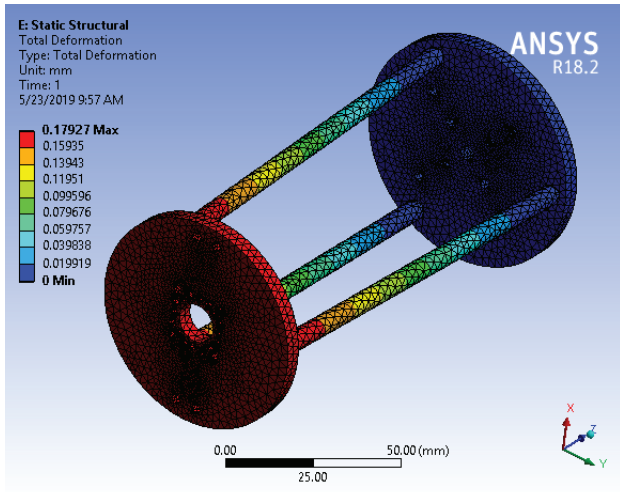
(j) Equivalent stress of forearm



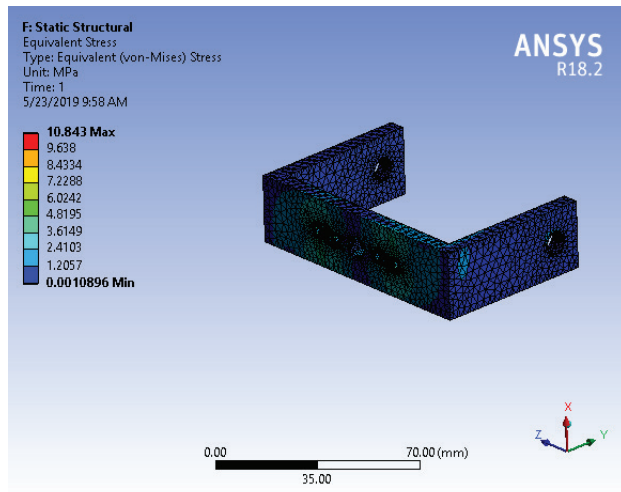
(h) Equivalent stress of elbow housing



(k) Deformation of shoulder clamp



(i) Deformation of forearm



(l) Equivalent stress of shoulder clamp

Fig. 8. Static Analysis results in ANSYS

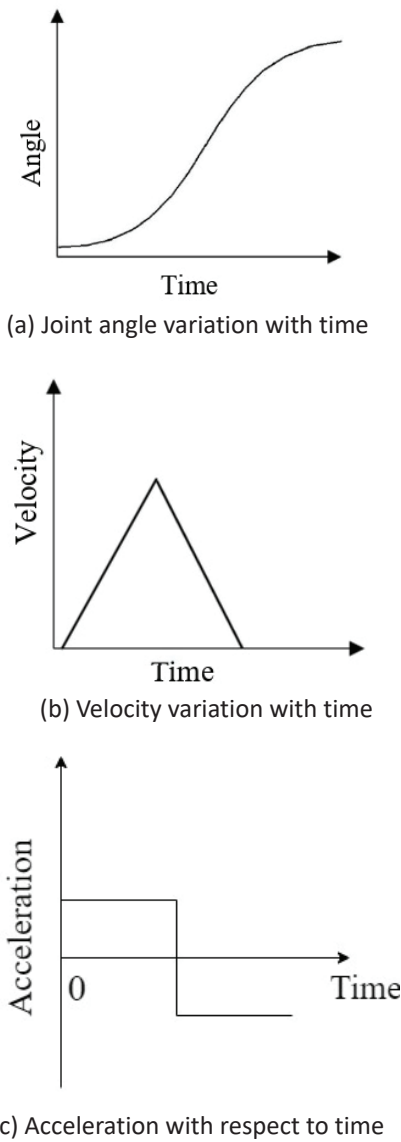


Fig. 9. Desired trajectory

3. Control Strategy of Robot

The dual arm robot is controlled from a computer and serial communication is implemented on the actuators which are connected using daisy chain setup. Position of the target is obtained with the help of image processing. Inverse kinematics is used to obtain the joint angles for the end effector to reach the target pose. The control architecture is shown in Fig. 10.

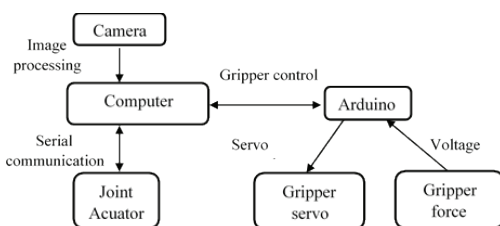


Fig. 10. Control architecture of dual arm robot

3.1. Target Acquisition

The target object is placed on a work plane of fixed height having a reference point of known pose. The relative position of the target object with respect to the reference point is obtained using image processing.

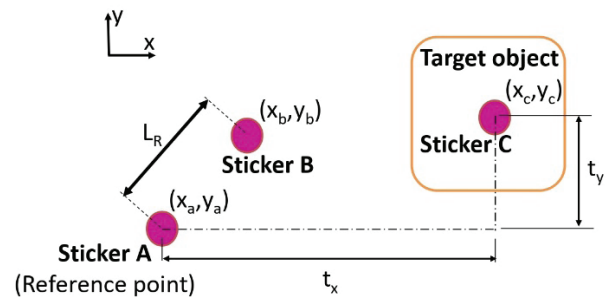


Fig. 11. Target position determination

In the work plane depicted in Fig. 11, sticker A is pasted at the reference point of a known pose in robot frame. Sticker B is pasted at a known distance from sticker A and sticker C is pasted on the target object. With the help of sticker colour, the coordinates of stickers in pixel dimensions are obtained using image processing. The scale factor f of the work plane is obtained from the equation (8), where L_R is the known real-world distance between sticker A and sticker B.

$$f = \frac{L_R}{\sqrt{(x_a - x_b)^2 + (y_a - y_b)^2}} \quad (8)$$

The relative position of the target object in x and y directions with respect to the reference point in real-world dimensions is obtained from the equations (9) and (10).

$$t_x = f \times (x_c - x_a) \quad (9)$$

$$t_y = f \times (y_c - y_a) \quad (10)$$

The procedure for the detection of stickers is explained in section 5.4.

3.2. Actuator Control

Closed loop feedback control is used for controlling the servo motors of dual arm robot joints (Fig. 12). An inbuilt PID controller is used for each joint actuator.

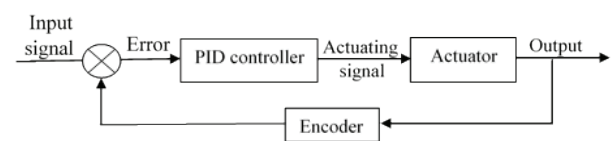


Fig. 12. Closed loop control

The hardware setup for actuator control is shown in Fig. 13. A computer is used as the main controller. Commands are communicated to the actuators using serial communication in Python environment.



Fig. 13. Hardware setup for Motor Control

4. Coordination of Dual Arm Robot

The dual arm robot has more dexterity and flexibility compared to a single manipulator arm to do coordinated tasks [13]. Coordination is achieved by determining the relative pose between the two end effectors. The motion planning and control for dual-arm coordination are the major hurdles in this stage. The task of transferring objects from one arm to the other is selected for demonstrating coordination between the two arms. The position of the target object on the work plane is obtained by image processing. The first arm approaches the object using inverse kinematics with the pose of the target object represented by transformation matrix 0T_t equated to the desired end effector pose ${}^0T_{11}$ as shown in equation (11).

$${}^0T_{11} = {}^0T_t \quad (11)$$

The configuration during the approach is shown in Fig. 14.

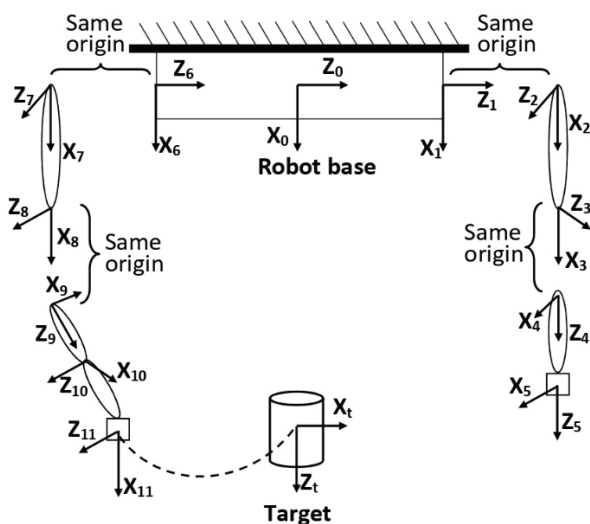


Fig. 14. Right arm of the dual arm robot approaching the target

4.1. Object Detection

Once the first arm grasps the object, it is then oriented in front of the robot camera to detect the object and to get its dimensional data for carrying out the coordinated tasks. Object detection is done using 2D image processing as it requires less computational power and is less expensive. Deep-learning based object detection is used with a trained database from which the object is identified and a bounding box is created around it. You Only Look Once (YOLO) ap-

proach is used for detecting the object [14], wherein it trains different images using bounding boxes, optimizes the detection and stores it in a database. Once the object is detected and its dimension is obtained in pixels from the bounding boxes, these dimensions are then further converted to real-world coordinate values using the scale factor used in target acquisition.

4.2. Task Implementation

To find the target pose for the second arm, a task dependent transformation T_R needs to be applied to the pose of the first arm end effector. The T_R is a function of the size of the bounding box (h) created from image detection and the target pose for the second arm 0T_5 is obtained using equation (12). The second arm is then approached towards the first arm to reach the target for manipulating the object.

$${}^0T_5 = {}^0T_{11}T_R \quad (12)$$

5. Results and Discussion

5.1. Workspace Plot

The workspace of the dual arm robot is plotted in MATLAB using the kinematic model developed. Monte Carlo method is used to plot the workspace of dual arm robot by providing the angle ranges for individual joints and plotting the corresponding end effector positions [15]. The plotted workspace of the dual arm robot is shown in Fig. 15.

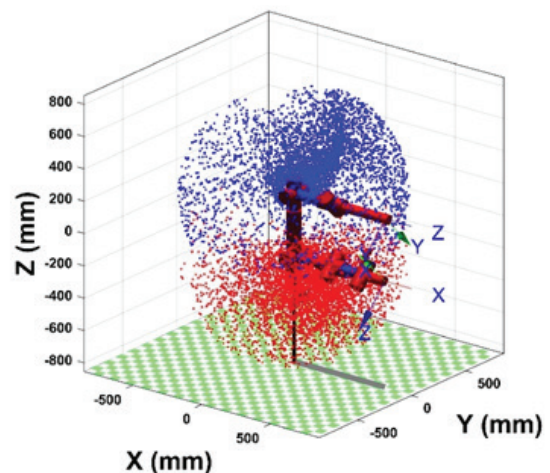


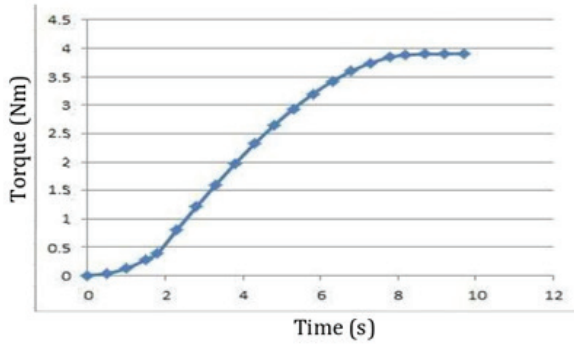
Fig. 15. Workspace Plot in MATLAB

5.2. Joint Torque Plots

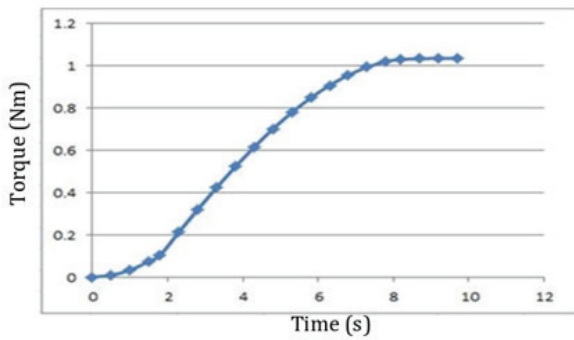
Joint torques are determined using L-E method as shown in Fig. 16. Maximum torques obtained at the shoulder joint is 4 Nm and at the elbow joint is 1 Nm.

The CAD model is imported and simulated in MSC ADAMS multibody dynamics software for validating the results obtained from L-E method. The results from software simulation are shown in Fig. 17. Maximum torque obtained at the shoulder joint is of 4.5 Nm

and at the elbow joint is 1.5Nm. The peak torque values from the mathematical model are agreeing with the simulation results and trend of variation of elbow and shoulder joints are almost same. Actuator selection is carried out by adding a FOS of 1.4 to the peak torque values. ROBOTIS Dynamixel MX-64T and MX-28T servo motors are selected for joint actuation by verifying the datasheets.

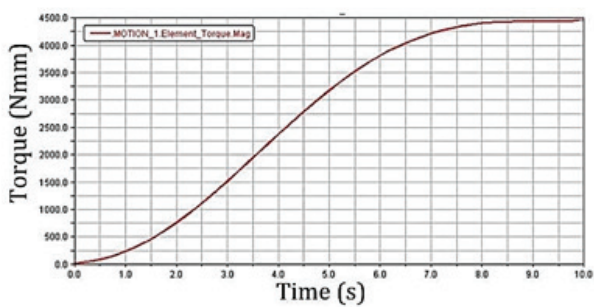


(a) Torque at shoulder joint

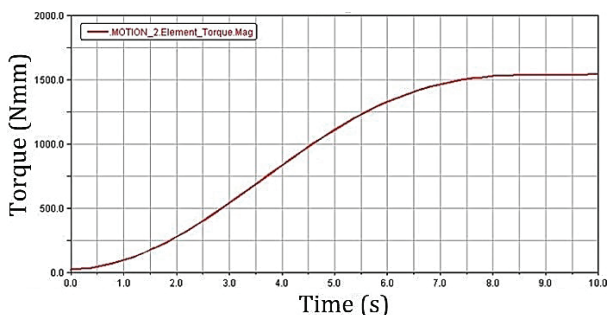


(b) Torque at elbow joint

Fig. 16. Matlab plot for joint torques by LE method



(a) Torque at shoulder joint

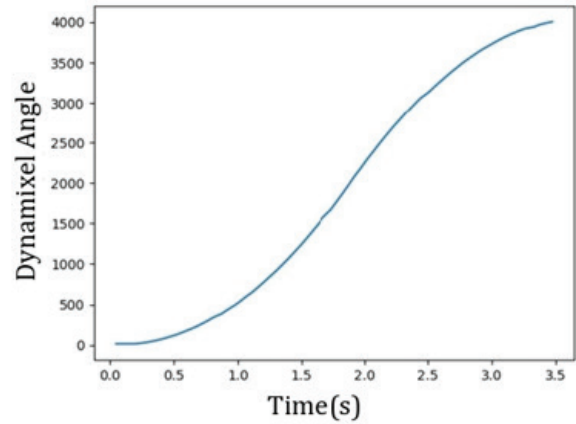


(b) Torque at elbow joint

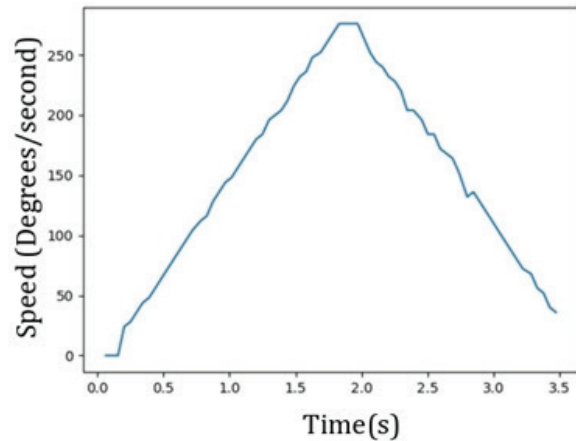
Fig. 17. ADAMS simulation results

5.3. Trajectory Generation

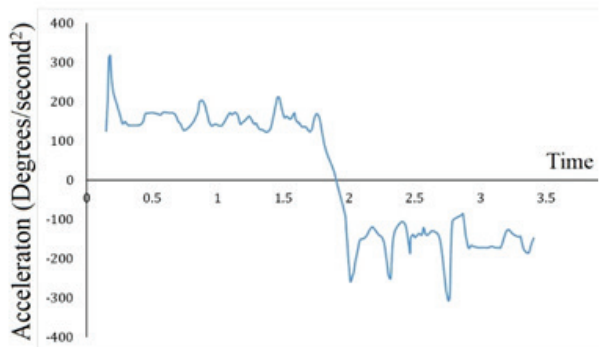
The proposed trajectory mentioned in section 2.4 is verified by plotting the velocity and position obtained from the encoder values of motors for arm roll motion. The plots are shown in Fig. 18.



(a) Angle variation with respect to time



(b) velocity profile with respect to time



(c) Acceleration profile

Fig. 18. Obtained joint trajectory

5.4. Target Detection

Target acquisition is tested by using a nut as the target object placed on the work plane using OpenCV [16,17]. A colour sticker is pasted on the nut and the position of the centre of the sticker is detected. The steps in image processing are shown in Fig. 19.

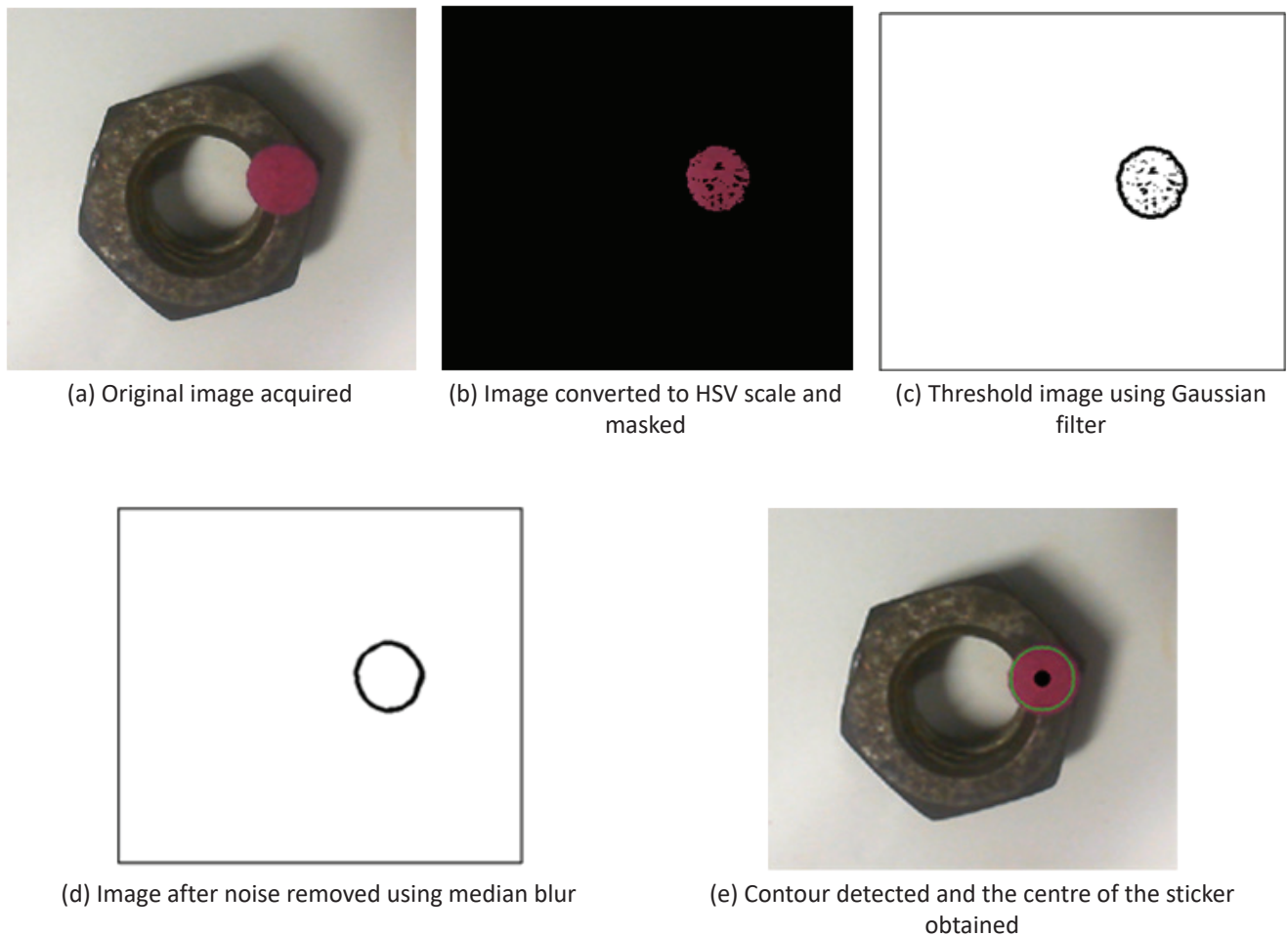


Fig. 19. Image processing algorithm

5.5. Joint Position Error

A trajectory for both arms to reach a point in the common workspace is selected for calculating joint position errors. Deviation from the desired joint angles is analysed using encoder values obtained from the Dynamixel motors. The desired and actual trajectories of both end effectors are plotted using MATLAB as shown in Fig. 20. The maximum error in joint angles for the given trajectory is recorded as 0.0276 radians which is at the right elbow joint. The error is due to the dimensional variations in fabricated parts and limited accuracy of the controller.

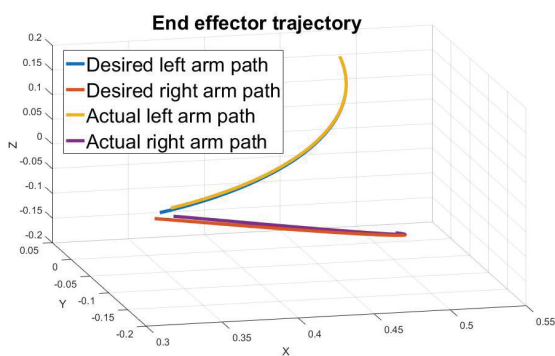


Fig. 20. Desired and actual trajectories of end effectors of dual arm robot

5.6. Experimentation

Experimentation is carried out on the fabricated system which is shown in Fig. 21. The designed gripper is 3D printed as shown in Fig. 22. The task tested is to detect the position and pick the object placed on the table using one arm, identify the object as bottle and obtain its dimensions (length and breadth of the bounding box). Then using equation (11) and equation (12), the other arm is approached towards the first to transfer the object. A Force Sensing Resistor (FSR) is attached to the gripping surface to limit the contact force.

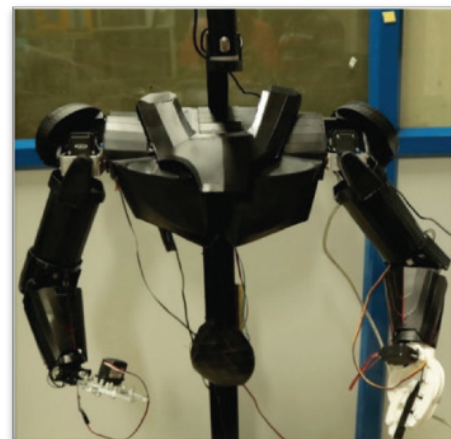


Fig. 21. Fabricated model of dual arm robot

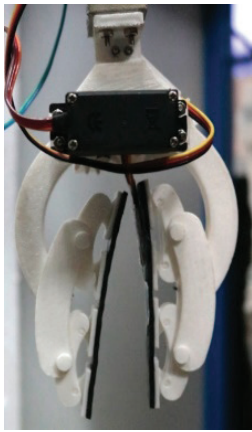
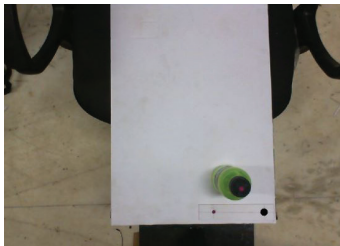


Fig. 22. 3D printed gripper

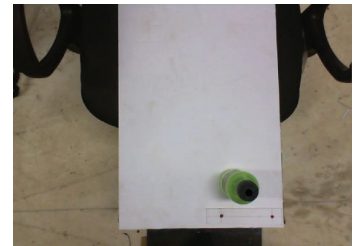
First, the position of the target object is obtained in pixel dimensions by image processing using OpenCV as explained in section 5.4. Two reference points at a known distance, are placed on the work plane to obtain the scale factor. The pose of one reference point on the work table is found using lead through programming. The position of the target object with respect to the base frame is calculated using the scale factor of the work plane.



(a) Detecting first reference point



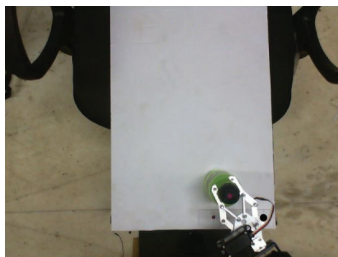
(b) Detecting second reference point



(c) Detecting target object position



(d) Obtaining the pose of first reference point by lead through method



(e) Grasping the target object



(f) Detecting the object



(g) Transferring object to the other hand

Fig. 23. Steps involved in the coordinated task



Fig. 24. Configuration for pouring water from bottle to cup

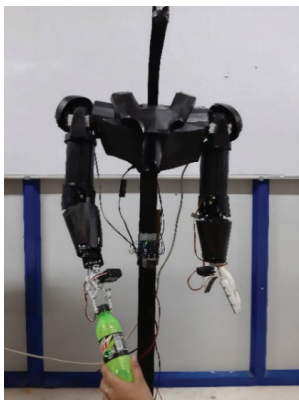


Fig. 25. Configuration for opening the cap of a bottle using roll motion

Using inverse kinematics, the end effector is moved towards the target object for manipulation. The robot camera images for steps involved in the coordinated task are shown in Fig. 23. The object is detected and bounding box is obtained. The length and breadth dimensions thus obtained are used to achieve the coordinated task as mentioned in section 4.2.

Other tasks tested on the dual arm robot include pouring liquid from bottle to cup and serving as shown in Fig. 24. Fig. 25 shows the robot opening the cap of the bottle for a person using the roll joint in the right arm. Thus the robot can be programmed to do tasks to help disabled people in doing their daily activities.

6. Conclusion and Future Scope

An anthropomorphic dual-arm robot capable of performing coordinated tasks with minimum degrees of freedom is developed. Closed loop control with PID is used for joint actuation. Target acquisition is carried out with the help of image processing. A gripper is designed for holding bodies of various shapes and sensors are integrated with it to limit the amount of force required to grasp an object. The basic coordinated task of transferring an object from one arm to another has experimented with the help of object detection. The compact anthropomorphic design and reduced cost make the proposed dual arm robot suitable for

aiding a disabled person for household activities. The dual arm robot can be attached to a mobile base to further extend the household application. Further improvement of coordination between the arms could be achieved in the developed model by integrating neural networks and machine learning in performing inverse kinematics. Electroencephalogram (EEG), speech recognition and eye movement detection can be incorporated to capture brain signals from humans to decide the required tasks. Target acquisition can be improved by extending the 2D work plane to 3D space. The dual arm robot can also be combined with Autonomous Underwater Vehicles (AUV), Drones, Space robots, etc. to operate in environments where direct human intervention is difficult.

ACKNOWLEDGEMENTS

This research work was supported financially by Research and Consultancy of National Institute of Technology Calicut, India (NITC/DEAN(R&C)/UG-RESEARCH-STRENGTHENING/2018). This support is gratefully acknowledged.

AUTHORS

Abhaykrishna K M – Department of Mechanical Engineering, National Institute of Technology Calicut, India, e-mail: abhaykrishnakm@gmail.com.

Nidhi Homey Parayil – Department of Mechanical Engineering, National Institute of Technology Calicut, India, e-mail: nidhihomey@gmail.com.

Ibin Menon Reghunandan – Department of Mechanical Engineering, National Institute of Technology Calicut, India, e-mail: ibinmenon57@gmail.com.

Sudheer A P* – Department of Mechanical Engineering, National Institute of Technology Calicut, India, e-mail: apsudheer@nitc.ac.in.

* Corresponding author

REFERENCES

- [1] J. Tarek, Z. Chiheb, M. Aref, "Modeling and Simulation of a Dual Arm Robot During the Compensation of an External Force", *Arabian Journal for Science and Engineering*, vol. 43, no. 9, 2018, 4713–4725
DOI: 10.1007/s13369-018-3089-2.
- [2] A. Banerji, R. Banavar, D. Venkatesh, "A Non-Dexterous Dual Arm Robot's Feasible Orientations Along Desired Trajectories: Analysis & Synthesis". In: *Proceedings of the 44th IEEE Conference on Decision and Control*, 2005, 4391–4396
DOI: 10.1109/CDC.2005.1582853.
- [3] P. Tsarouchi, S. Makris, G. Michalos, M. Stefanos, K. Fourtakas, K. Kaltsoukalas, D. Kontrovakis, G. Chryssolouris, "Robotized Assembly Process Using Dual Arm Robot", *Procedia CIRP*, vol. 23, 2014, 47–52
DOI: 10.1016/j.procir.2014.10.078.

- [4] Y. Huang, S. Li, S. Li, Y. Ke, "Design and Implementation of Dual-Arm Robot with Homogeneous Compliant Joint". In: *2017 9th International Conference on Intelligent Human-Machine Systems and Cybernetics (IHMSC)*, vol. 2, 2017, 265–270
DOI: 10.1109/IHMSC.2017.172.
- [5] D. Lee, H. Park, J. Park, M. Baeg, J. Bae, "Design of an anthropomorphic dual-arm robot with biologically inspired 8-DOF arms", *Intelligent Service Robotics*, vol. 10, no. 2, 2017, 137–148
DOI: 10.1007/s11370-017-0215-z.
- [6] C. Park, K. Park, "Design and kinematics analysis of dual arm robot manipulator for precision assembly". In: *2008 6th IEEE International Conference on Industrial Informatics*, 2008, 430–435
DOI: 10.1109/INDIN.2008.4618138.
- [7] "ABB's Collaborative Robot – YuMi – Industrial Robots From ABB Robotics". <https://new.abb.com/products/robotics/industrial-robots/irb-14000-yumi>. Accessed on: 2020-03-10.
- [8] D. A. Winter, *Biomechanics and Motor Control of Human Movement*, John Wiley & Sons, Inc., 2009.
- [9] R. K. Mittal, I. J. Nagrath, *Robotics and Control*, Tata Mc Graw-Hill, 2003.
- [10] T. F. Coleman, Y. Li, "On the convergence of interior-reflective Newton methods for nonlinear minimization subject to bounds", *Mathematical Programming*, vol. 67, no. 1, 1994, 189–224
DOI: 10.1007/BF01582221.
- [11] R. Budynas, K. Nisbett, *Shigley's Mechanical Engineering Design*, McGraw-Hill Education, 2014.
- [12] J. J. Craig, *Introduction to Robotics: Mechanics and Control*, Pearson, 2004.
- [13] T. Liu, Y. Lei, L. Han, W. Xu, H. Zou, "Coordinated Resolved Motion Control of Dual-Arm Manipulators with Closed Chain:", *International Journal of Advanced Robotic Systems*, vol. 13, no. 3, 2016
DOI: 10.5772/63430.
- [14] J. Redmon, S. Divvala, R. Girshick, A. Farhadi, "You Only Look Once: Unified, Real-Time Object Detection". In: *2016 IEEE Conference on Computer Vision and Pattern Recognition (CVPR)*, 2016, 779–788
DOI: 10.1109/CVPR.2016.91.
- [15] K. Shengzheng, H. Wu, L. Yao, D. Li, "Coordinated workspace analysis and trajectory planning of redundant dual-arm robot". In: *2016 13th International Conference on Ubiquitous Robots and Ambient Intelligence (URAI)*, 2016, 178–183
DOI: 10.1109/URAI.2016.7625731.
- [16] G. Bradski, A. Kaehler, *Learning OpenCV. Computer Vision with the OpenCV Library*, O'Reilly Media, Inc., 2008.
- [17] A. Sanin, C. Sanderson, B. C. Lovell, "Shadow detection: A survey and comparative evaluation of recent methods", *Pattern Recognition*, vol. 45, no. 4, 2012, 1684–1695
DOI: 10.1016/j.patcog.2011.10.001.